Journal of Nuclear Medicine, published on May 18, 2017 as doi:10.2967/jnumed.117.193268

Imaging of programmed death ligand-1 (PD-L1): impact of protein concentration on distribution of anti-PD-L1 SPECT agent in an immunocompetent melanoma murine model

Jessie R. Nedrow, Anders Josefsson, Sunju Park, Sagar Ranka, Sanchita Roy, and George Sgouros

Russell H. Morgan Department of Radiology & Radiological Science

Johns Hopkins University School of Medicine

Baltimore, MD, USA

Running title: Factors impacting anti-PD-L1 agents

Financial Support: NIH RO1CA187037

Corresponding author:

Dr. George Sgouros

Russell H. Morgan Department of Radiology & Radiological Science

Johns Hopkins University School of Medicine

Phone: 410-614-0116

Fax: 413-487-3753

CRBII 4M.61, 1550 Orleans Street

Baltimore MD, 21231, USA

Email: gsgouros@jhmi.edu

First Author:

Dr. Jessie R Nedrow

Russell H. Morgan Department of Radiology & Radiological Science

Johns Hopkins University School of Medicine

Phone: 410-614-0254

CRBII 4M.62, 1550 Orleans Street

Baltimore MD, 21231, USA

ABSTRACT

Programmed cell Death Ligand 1 (PD-L1) is part of an immune checkpoint system that is essential for preventing autoimmunity and cancer. Recent approaches in immunotherapy targeting immune checkpoints have shown great promise in a variety of cancers, including metastatic melanoma. The use of targeted molecular imaging would help identify patients who will best respond to anti-PD-L1 treatment while potentially providing key information to limit immune-related adverse effects (irAEs). Recently, we developed an antibody based PD-L1-targeted imaging agent to identify PD-L1 positive tumors *in vivo*. To further understand how to best use these new PD-L1-targeted imaging agents it is important, as a first step, to understand how the signal is affected by different parameters.

Method*:* We evaluated the impact of protein concentration on the distribution of ^{111}In-DTPA-anti-PD-L1-BC, an ^{111}In-antibody conjugate targeted to PD-L1, in an aggressive mouse melanoma model.

Results*:* ^{111}In-DTPA-anti-PD-L1 (K_d=0.6±0.1 nM) demonstrated increased uptake in the B16F10 tumor at protein concentrations ≥ 1 mg/kg at 24 hrs and ≥ 3 mg/kg at 72 hrs. At 24 hrs the PD-L1 rich spleen and lungs demonstrated decreasing uptake with increasing protein concentration. At 72 hrs uptake in the thymus was significantly increased at protein concentrations ≥ 3mg/kg. Both time points demonstrated increased tracer amounts remaining in circulation as the amount of cold antibody was introduced.

Conclusion: These studies demonstrate that ^{111}In-DTPA-anti-PD-L1 is capable of identifying tumors that overexpresses PD-L1, as well as monitor the impact of PD-L1 rich organs on the distribution of anti-PD-L1 antibodies.

Key words: anti-PD-L1, SPECT, melanoma, targeted antibodies, immune checkpoint inhibitors

INTRODUCTION

Melanoma is the most dangerous form of skin cancer. It represents only one percent of skin cancer patients, but once metastasized, it is responsible for the majority of skin cancer deaths. Treatment options for metastatic melanoma are severely limited, but recent approaches in immunotherapy targeting immune checkpoints have shown great promise in a variety of cancers, including melanoma (*1*-*3*).

Programmed cell Death Ligand 1 (PD-L1) is part of an immune checkpoint system, which is essential for preventing autoimmunity and cancer (*4*). PD-L1 expression is found on a variety of immune cells and is also found in immune-cell rich organs, such as, the spleen and thymus (*5*-*7*). Tumor cells have developed the ability to co-opt these immune checkpoints to suppress anti-tumor immunity. Immune checkpoint therapy, such as anti-PD-L1 therapy, targets inhibitory checkpoint signaling, allowing the body's immune system to recognize tumor cells and mount an attack against them. PD-L1 overexpression in tumor cells is associated with a poorer prognosis, but patients whose tumors exhibit overexpression typically have a stronger response to anti-PD-L1 therapy (*8*). PD-L1-expression in tumor-infiltrating immune cells has also been associated with a stronger response to immune checkpoint inhibition therapy than PD-L1-postivity in the tumor itself (*9*). However, mixed responses to immune checkpoint therapy and the development of immune-related adverse events (irAEs) have highlighted a deficiency in the current methods to evaluate and monitor patients for anti-PD-L1 treatment.

In clinical trials patients identified by immunohistochemistry (IHC) to overexpress PD-L1 in advanced melanoma have a 39% response rate to anti-PD-L1 therapy, compared to a 13% response rate in patients with PD-L1 negative melanoma (*8*). IHC is limited to a snap shot of the tumor microenvironment and is unable to capture the dynamic nature of PD-L1 expression in the tumor or PD-L1 rich organs. The clarification of PD-L1 status via molecular imaging is necessary to address why a 13% response rate was seen in patients with negative PD-L1 status. In addition, irAEs have been noted in patients receiving anti-PD-L1 therapy, with 5% of patients experiencing grade 3 or 4 irAEs (*2*). The recent exploration of the combination of immunotherapies has shown significant improvement in treatment efficacy, as well as significant increases in high-grade irAEs (*10,11*). Furthermore, increases of irAEs are anticipated as the patient population receiving immune checkpoint therapies is expected to expand due to the success of immunotherapies in the clinic. A thorough understanding of the distribution of the therapeutic anti-PD-L1 antibody within the whole body would provide valuable insight to help answer the following questions: 1) Will a patient respond to anti-PD-L1 therapy? 2) Would determining a dose based on individual patients help increase a patient's likelihood to respond? 3) Would monitoring PD-L1 expressing in immune-cell rich organs help identify patients that are at risk for developing irAEs?

We have previously reported the development and evaluation of an anti-PD-L1 SPECT agent in an immune intact murine model of breast cancer, resulting in high uptake in the PD-L1 positive tumor but also immune-associated organs,

such as the thymus and spleen (*12*). This study demonstrated the feasibility of developing antibody-based anti-PD-L1 SPECT molecular imaging agents capable of identifying PD-L1 expressing tumors, and highlighted the significant impact of the spleen and thymus on the distribution of anti-PD-L1 antibodies. To understand how to best use PD-L1-targeted imaging agents to answer the above mention questions, it is important, as a first step, to understand how the signal is affected by different parameters. In this work, we used an immunocompetent melanoma murine model to examine how the amount of antibody administered affects the signal obtained, specifically focusing on the impact of immune-related organs on the delivery of labeled and unlabeled anti-PD-L1 antibodies to reach the tumor site. We accomplished this by investigating the impact of protein concentration on the distribution of the anti-PD-L1 SPECT agent, ^{111}In-DTPA-labeled antibody (anti-PD-L1-BC), at a tracer amount as well as co-administered with unlabeled anti-PD-L1 at therapeutic amounts, providing a theranostic approach. ^{111}In-DTPA-anti-PD-L1-BC was evaluated in an immunocompetent murine model of melanoma via *in vivo* SPECT imaging and *ex vivo* biodistribution studies. The results were consistent with our previous work, again highlighting the impact of immune-associated organs including the thymus and spleen, on the distribution of ^{111}In-DTPA-anti-PD-L1-BC. Furthermore, this work provided additional insights on the significance of these immune-associated organs, and also identified additional PD-L1 rich organs that impact the distribution of anti-PD-L1 antibodies.

MATERIALS AND METHODS

Reagents

All chemicals were purchased from Sigma-Aldrich Chemical Co. (St. Louis, MO, USA) or Thermo Fisher Scientific (Pittsburgh, PA, USA), unless otherwise specified. Aqueous solutions were prepared using ultrapure water (resistivity, 18 MΩ·cm) treated with Chelex resin purchased from Bio-Rad Laboratories, Inc. (Berkeley, CA, USA). p-SCN-Bn-DTPA was purchased from Macrocyclics, Inc. (Dallas, TX, USA). Indium-111 ($[^{111}In]InCl_3$) was purchased from MDS Nordion (Vancouver, BC, Canada). The *in vivo* plus anti-mouse PD-L1 antibody was purchased from Bio X Cell (West Lebanon, NH, USA). The murine melanoma cell line, B16F10, was kindly provided by Dr. Carolyn Anderson at the University of Pittsburgh, and was authenticated by IDEXX bioresearch (Westbrook, ME, USA). The murine lymphoma cell line, EL4.murineByH1 (EL4), was obtained from Ampliummune, Inc (Gaithersburg, MD, USA). See supplemental material for cell growth conditions.

Radiolabeling of DTPA-anti-PD-L1-BC antibodies with ^{111}In

The radiolabeled anti-PD-L1-BC antibody was prepared as previously described (*12*). See supplemental materials for experimental details.

In vitro studies

Western Blot Analysis.

Western Blots were performed on cell lysates incubated with and with INF-γ as previously described (*12*); as well as selected organs collected from C57BL/6 mice. See supplemental materials for experimental details.

Flow cytometry.

Flow cytometry was performed as previously described (*12*). Preparation of the EL4, a positive control, and B16F10 murine cell lines were done in parallel to maintain the same treatment conditions. See supplemental materials for experimental details.

Binding assay.

The binding affinity of ^{111}In-DTPA-anti-PD-L1-BC was determined in B16F10 cells as described previously with modification (*12,13*). See supplemental materials for experimental details.

In vivo studies

Animals.

Seven to eight week old female C57BL/6 mice from Charles River Laboratories (Frederick, MD, USA) were used in this study. All animal studies were approved by the Animal Care and Use Committee of the Johns Hopkins University School of Medicine. For B16F10 tumors, mice were injected subcutaneously in the right flank (biodistribution) or shoulder (SPECT imaging) with 10^6 cells in PBS. It should be noted that C57BL/6 mice with B16F10 cells subcutaneously implanted

in their ear have been shown to develop spontaneous lung metastasis in approximately a third of the mice after a 4-week growth period (*14*). However, lung metastatic models having B16F10 injected directly to the lungs via the tail vein only show early signs of lung metastases at approximately two-weeks post-injection (*15*).

SPECT imaging of ^{111}In-DTPA-anti-PD-L1-BC in B16F10 tumor bearing C57BL/6 mice.

Tumor bearing healthy C57BL/6 female mice were injected intravenously (i.v.) with 15–16 MBq ^{111}In-DTPA-anti-PD-L1 (60 µg) 10-days post B16F10 cell injections. The mice (n=2) were imaged at 1, 24 and 72 hrs post-injection (p.i.) of ^{111}In-DTPA-anti-PD-L1 with the VECTor^4 SPECT imaging system (MILabs, Utrecht, The Netherlands) using a general-purpose mouse collimator, with 0.6 mm pinholes yielding a 0.4 mm resolution in the reconstructed images. Images were acquired for 60 min at the 1 and 24 hr time points, and for 90 min at the 72 hrs time point. Images were reconstructed with voxel side length 0.2 mm using POS-EM (*16*), a vendor supplied iterative algorithm. SPECT images were analyzed with the software ImageJ Fiji version 1.49b (NIH; Bethesda, MD, USA) and the voxel intensity was calibrated using images of a standard with a known activity and volume. Co-registration of CT and SPECT for anatomical reference was completed using AMIDE software (http://amide.sourceforge.net).

Biodistribution of ^{111}In-DTPA-anti-PD-L1-BC in B16F10 tumor bearing C57BL/6 mice.

Biodistribution experiments were conducted as previously described with minor modifications (*13,17,18*). Briefly, healthy B16F10 tumor-bearing female C57BL/6 mice (n=5/time point) were injected i.v. with ^{111}In-DTPA-anti-PD-L1-BC (0.37 MBq, 0.2 antibody protein [mg]/mouse mass [kg]) 10 days post B16F10 cell injections. At 1, 24, 72, and 96 hrs p.i. of ^{111}In-DTPA-anti-PD-L1-BC the mice were sacrificed. The blood, heart, lungs, liver, kidneys, spleen, stomach (with content), intestine (with content), bone, thymus, muscle, and tumors were harvested, weighed, and measured in a gamma well counter. In addition, B16F10 tumor bearing C57BL/6 mice were injected i.v. with ^{111}In-DTPA-anti-PD-L1-BC (0.37 MBq) at the following concentrations: 0.65, 1.0, 3.0, 5.0, and 10.0 mg/kg. Mice were sacrificed at 24 and 72 hrs p.i., organs were visually inspected, harvested and processed as described above. The percent-injected dose per gram (%ID/g) was calculated by comparison to a weighed, diluted standard.

Statistical analysis

Statistical analysis was performed using the software, GraphPad PRISM 6 (La Jolla, CA, USA). All data are presented as the mean value ± standard deviation. Groups were compared using two-way ANOVA; values were considered significant if ≤ 0.05.

RESULTS

Radiolabeling

The ^{111}In-DTPA-anti-PD-L1-BC conjugate was radiolabeled in 45-60 min at room temperature in ammonium acetate buffer at an average specific activity of 21.2 ± 1.97 MBq/nmol with >95% radiochemical purity following purification.

Western Blot Analysis

A western blot analysis was performed to evaluate PD-L1 expression in B16F10 cells. The EL4 cell line served as a positive control line. The PD-L1 expression levels with and without IFN-□ were normalized to β-actin (PD-L1/β-actin). The B16F10 cells were positive for PD-L1 expression, having similar levels with or without IFN-□□□**Supplemental Figure 1**) □□In non-tumor bearing C57BL/6 mice the thymus, spleen, lungs, and kidneys showed PD-L1 expression, while the liver had very low to no expression. PD-L1 expression levels (PD-L1/ β-actin) for the liver were set to 1 and relative expression levels were determined in the thymus (4.85), Spleen (3.87), lung (3.22), and kidneys (1.67)[**Supplemental Fig. 2**].

Flow cytometry

Cell-surface expression of PD-L1 with and without IFN-γ treatment was also evaluated by flow cytometry (**Fig. 1**). PD-L1 expression on the EL4 cell line was not significantly increased with IFN-γ treatment. PD-L1 expression on the B16F10 cells increased 4.1-fold with IFN-γ incubation as determined by the mean fluorescent intensity (MFI). Response to IFN-γ highlights the ability of the

B16F10 tumor cell line to mount an anti-immunity response to immune cell signaling.

Receptor Binding Assay

Saturation binding assay shows that ^{111}In-DTPA-anti-PD-L1-BC binds with high affinity to PD-L1, having a K_d of 0.58 ± 0.06 nM (**Supplemental Fig. 3)**.

In vivo studies

Biodistribution of ^{111}In-DTPA-anti-PD-L1-BC.

Biodistribution studies were carried out in C57BL/6 female mice bearing B16F10 tumors at 1, 24, 72, and 96 hrs p.i. of ^{111}In-DTPA-anti-PD-L1-BC (specific activity = 21.3 MBq/nmol, approximately 0.13 mg/kg, **Fig. 2**). At 1 h, the highest uptake was observed in the blood, lung, liver, spleen, and kidneys. The tumor demonstrated the greatest uptake at 24 hrs p.i. (6.6 ± 3.1 %ID/g) with a tumor to muscle ratio of 4.6 ± 2.0, and a tumor to blood ratio of 4.2 ± 1.5. This uptake was lower than our previously reported work in a murine model of breast cancer, most likely due to the use of a different anti-PD-L1 antibody that is no longer available to us. Following its peak at 24 hrs the tumor uptake decreased at 72 and 96 hrs. The uptake in the kidneys had a similar pattern as the tumor, with a peak at 24 hrs followed by decreasing uptake. Decreasing uptake over the 96 hrs window was also shown in the blood, lungs, and spleen; significant decreases (p-value ≤ 0.05) were seen in both the lungs and spleen.

To examine the impact of a wider range of administered antibody, additional biodistribution studies were performed using ^{111}In-DTPA-anti-PD-L1-BC (0.37 MBq) antibody doses of approximately 0.5-0.6 mg/kg (Dose 1), 1 mg/kg (Dose 2), 3 mg/kg (Dose 3), 5 mg/kg (Dose 4), and 10 mg/kg (Dose 5). At 24 hrs the blood, lungs, spleen, and tumor had significant changes in uptake due to the increasing dose concentration (**Fig. 3**). The presence of additional unlabeled antibody in the administered doses, demonstrated decreased uptake in the lung and spleen, and increased uptake in the tumor and blood. The highest uptake in the tumor was observed at Dose 3 (11.9 ± 3.0 %ID/g) with tumor to muscle ratio of 10 ± 0.2, and a tumor to blood ratio of 1.0 ± 0.2 (**Table 1**). At 72 hrs the uptake in the lungs remained consistent over the doses, but significant changes were seen again in the blood, spleen, and tumor, as well as in the thymus (**Fig. 3**). The blood, tumor, and thymus uptake increased with doses having higher amounts of cold antibody, while the spleen uptake decreased. The highest uptake in the tumor occurred at Dose 5 (15.4 ± 7.9 %ID/g), with tumor to muscle ratio of 8.7 ± 2.8, and a tumor to blood ratio of 1.9 ± 1.0 (**Table 2**). Visual inspection of the organs in the *ex vivo* biodistributions presented here showed no signs of metastatic disease. The increase in dose from 0.6-10 mg/kg is representative of a competitive blocking experiment. For traditional blocking experiment we would expect to observe a decrease in tumor uptake, indicating selective binding to the target. However, these results are not seen due to the spleen serving as a sink for the PD-L1 antibody. The significant decreases in spleen uptake at 24 hours as well as at 72 hours for the 10 mg/kg dose is indicative of selective binding of

the labeled and unlabeled PD-L1 antibody to PD-L1 due to the high presence of PD-L1 positive immune cells found in the spleen. The improved tumor uptake is attributed to excess antibody occupying sites in the spleen, allowing more labeled antibody to reach the tumor following passage through the spleen.

SPECT imaging of ^{111}In-DTPA-anti-PD-L1-BC.

Whole body SPECT images were collected at 1, 24, and 72 hrs p.i. of ^{111}In-DTPA-anti-PD-L1-BC. At 1 hr the majority of activity was concentrated along the major arteries (carotids, caudal, and femoral), and heart. The lungs demonstrated modest contrast to background. The spleen, liver, and tumor were distinguishable, but had low contrast to background. At 24 hrs (**Fig. 4**), clearance from the blood reduced the signal so that only the carotids and heart had modest to low contrast to background. The B16F10 isograft had the highest contrast to background, and was clearly visible. The liver and spleen were defined with superior contrast to background as well. The thymus (**Supplemental Fig. 4**) as well as the brown adipose tissue (BAT, **Supplemental Fig. 5**) had modest contrast to the background. At 72 hr the liver, spleen, and tumor isograft are distinct with modest contrast to the background. Due to the rapid growth of the B16F10 tumor line, the isograft is significantly larger at 72 hrs than at 24 hrs, obstructing the visualization of the BAT. The low signal to noise at 72 hrs does not allow for a clear definition of the thymus (Supplemental Fig. 6).

DISCUSSION

Anti-PD-L1 antibodies are active against a variety of cancers, but have an unpredictable success rate. The amount of antibody that is currently administered for patient therapy was empirically determined in multi-arm, phase 1 trials (*2*). Based on these results the amount of antibody is administered to all patients on a per kg basis regardless of tumor burden or PD-L1 expression. The ability to accurately determine PD-L1 expression and monitor the distribution of anti-PD-L1 antibodies could enable a precision medicine approach to immune checkpoint inhibition therapy. Before such an approach may be implemented, a greater understanding of the biodistribution of such therapeutics is required, as well as a detailed understanding of how normal organ distribution is impacted by the amount of antibody administered. Our previous work demonstrated the feasibility of modifying an anti-PD-L1 antibody to deliver a SPECT imaging payload to PD-L1-positive sites, including a subcutaneous breast cancer tumor (*12*). In this work we examine the effects of antibody concentration on the distribution of the anti-PD-L1 SPECT agent in a mouse model of melanoma.

The preliminary biodistribution was evaluated at a specific activity 21.3 MBq/nmol (4 μg). The results show high uptake in the spleen, which serves as a sink for the anti-PD-L1 antibody, resulting in minimal uptake in the tumor. To enhance the uptake in the tumor we evaluated ^{111}In-DTPA-anti-PD-L1 combined with unlabeled anti-PD-L1 antibody at therapeutic doses to help block PD-L1 sites in the spleen. We selected the 24 and 72 hrs time points based upon the preliminary biodistribution study of ^{111}In-DTPA-anti-PD-L1-BC in the described melanoma mouse model at tracer amounts and on results obtained from our

previous studies in a breast cancer mouse model (*12*). Co-administration of the unlabeled antibody with ^{111}In-DTPA-anti-PD-L1-BC effectively lowered the specific activity by increasing the amount of antibody protein administered, providing an agent capable of both diagnostic and therapeutic applications. The resulting agent allows for a theranostic approach to guide and optimize anti-PD-L1 therapy potentially by relating observed effects to the distribution of the anti-PD-L1 antibody. The *ex vivo* biodistribution of ^{111}In-DTPA-anti-PD-L1-BC was consistent with our previous observations in the breast cancer model demonstrating that the spleen serves as a sink with uptake associated with PD-L1+ B-cells, splenic dendritic cells, and macrophages (*7*); and uptake in the thymus is not significantly affected by increasing protein amounts at the 24-hr time point. However, the current study provides additional insights into the effects of protein concentration on the distribution of anti-PD-L1 antibodies. First, the uptake in the thymus increased at the later time point with doses containing higher protein concentrations (≥ 3 mg/kg). Secondly, at the early time point uptake in the lungs was significantly blocked as the protein concentration was increased. Finally, a dose of 3 mg/kg appears to provide optimal distribution of the anti-PD-L1 antibody in the described mouse model of melanoma. At this dose, uptake in the tumor is comparable to the higher doses, but the concentration in the blood is not increased to the same extent as at higher dose levels.

The thymus having a PD-L1 rich environment due to its association with naïve T-cell output is impacted by immune checkpoint therapy (*6*). In normal

thymus tissue PD-L1 expression is associated with the epithelial cells (*19*). Immune checkpoint therapy, including anti-PD-L1 therapy, has been associated with adverse effects, such as, myasthenia gravis has been seen in a small percent of patients receiving anti-PD-L1 therapy (*2*). However, the recent report of fatal nivolumab-related myasthenia gravis has further stressed the need to understand the impact of immune checkpoint therapy on the thymus (*20*). In addition, the impact of uptake in the thymus may vary due to variation in activity between patients, especially in pediatric cancer patients. The translation of anti-PD-L1 therapy to pediatric cancer would require a better understanding of the thymus' impact on the distribution of these antibodies since the thymus activity decreases with age, potentially contributing to increased susceptibility to infection, autoimmune disease, and cancer (*21*). The data presented here highlight a significant increase in thymus uptake of the labeled anti-PD-L1 antibody between the doses administered. Specifically, the doses with increased protein concentration (≥3 mg/kg) demonstrated increased uptake over time of the labeled anti-PD-L1 antibody, having the highest uptake occur at the latter time point. However, there were not significant differences in uptake between doses ≥3 mg/kg, suggesting saturation of binding sites in the thymus occur at the 3-mg/kg dose.

The lung is host to a variety of immune cells due to its continuous exposure to external pathogens (*22*). PD-L1 expression in the lungs is associated with resident immune cells, particularly alveolar macrophages (*23,24*). Adverse effects including pneumonitis, influenza-like illnesses, and sarcoidosis highlight

the need to have a clear understanding of the distribution and impact of immune checkpoint therapies on non-tumor sites, such as, the lungs (*2*). This study highlighted differences in lung uptake of ^{111}In-DTPA-anti-PD-L1-BC at the early time point. Specifically, as the concentration of unlabeled antibody increased, binding sites for ^{111}In-DTPA-anti-PD-L1-BC decreased at the 24 hrs time point. There was not a significant difference of ^{111}In-DTPA-anti-PD-L1-BC uptake between the doses administered in the lungs at the later time point. This is suggestive that the PD-L1 binding sites in the lungs were saturated at doses ≥3 mg/kg at 24 hrs and all doses at 72 hrs.

Whole-body SPECT images of ^{111}In-DTPA-anti-PD-L1-BC at the determined optimal dose (3 mg/kg) are supportive of the biodistribution data. The SPECT imaging demonstrated that tumor, spleen, and liver are clearly defined at the later time points. At the 24 hrs time point intensified signal was noted in the location of the thymus, which is consistent with our biodistribution data. The development of an imaging agent for PET imaging with a higher resolution and sensitivity would be beneficial in distinguishing the thymus. Hettich, et al. demonstrated that with an anti-PD-L1 PET agent they were able to clearly identify uptake in the BAT in C57BL/6 mice, relating to CD45+ leukocytes (macrophages and CD3+ T-cells) (*25*). The SPECT images of ^{111}In-DTPA-anti-PD-L1-BC were able to distinguish the BAT in the murine model of melanoma. In addition, we confirmed uptake in the BAT in a murine model of breast cancer as well in biodistribution studies (unpublished data).

The optimal dose was determined to be 3-mg/kg for the described murine model of melanoma. Melanoma has been recognized to be immunogenic and responsive to immune checkpoint therapies compared to other cancers. The optimal dose may vary between other cancer types that are less immunogenic and responsive to immune checkpoint therapies. Also, it is likely that the optimal per body weight amount of anti-PD-L1 Ab will be different in humans than in mice. The approach presented in this work, provides a means to identify disease-specific optimal amounts. The development of anti-PD-L1 theranostic agents and imaging protocols is critical in providing a personalized approach to immune checkpoint therapies.

CONCLUSION

We demonstrated the dependence of PD-L1 antibody biodistribution on the amount of antibody administered and identify an optimal antibody level that maximizes tumor delivery relative to normal organs in a mouse model of melanoma. We also confirm that the spleen is a significant sink for PD-L1 antibody and that the amount available in the tumor environment is impacted by splenic uptake. Furthermore, we demonstrated the impact of the dose concentration on the distribution of the anti-PD-L1 antibody to the thymus and lungs. Anti-PD-L1 imaging has substantial potential for adjusting administered anti-PD-L1 antibody to optimize treatment, evaluate the patient-specific variability in antibody distribution to ensure adequate amounts of antibody reach tumor

sites, identify development of adverse effects, and better understand why response to this type of therapy is variable across different patients.

ACKNOWLEDGMENTS

We'd like to thank Drs. Elizabeth Jaffe, Suzanne Topalian, and Leisha Emens for their helpful insights on PD-L1 therapy. Drs. Ben Tsui, Andew Rittenbach and Taek-Soo Lee for their assistance with the small-animal SPECT imaging.

Supported by NIH RO1CA187037

REFERENCES

1. Lipson EJ, Forde PM, Hammers HJ, Emens LA, Taube JM, Topalian SL. Antagonists of PD-1 and PD-L1 in cancer treatment. *Semin Oncol.* 2015;42:587-600.

2. Brahmer JR, Tykodi SS, Chow LQ, et al. Safety and activity of anti-PD-L1 antibody in patients with advanced cancer. *N Engl J Med.* 2012;366:2455-2465.

3. Larkin J, Chiarion-Sileni V, Gonzalez R, et al. Combined nivolumab and ipilimumab or monotherapy in untreated melanoma. *N Engl J Med.* 2015;373:23-34.

4. Pardoll DM. The blockade of immune checkpoints in cancer immunotherapy. *Nat Rev Cancer.* 2012;12:252-264.

5. Carter L, Fouser LA, Jussif J, et al. PD-1:PD-L inhibitory pathway affects both CD4(+) and CD8(+) T cells and is overcome by IL-2. *Eur J Immunol.* 2002;32:634-643.

6. Murray JM, Kaufmann GR, Hodgkin PD, et al. Naive T cells are maintained by thymic output in early ages but by proliferation without phenotypic change after age twenty. *Immunol Cell Biol.* 2003;81:487-495.

7. Liu Q, Lu JY, Wang XH, Qu BJ, Li SR, Kang JR. Changes in the PD-1 and PD-L1 expressions of splenic dendritic cells in multiple-organ dysfunction syndrome mice and their significance. *Genet Mol Res.* 2014;13:7666-7672.

8. Herbst RS, Soria JC, Kowanetz M, et al. Predictive correlates of response to the anti-PD-L1 antibody MPDL3280A in cancer patients. *Nature.* 2014;515:563-567.

9. Kim MY, Koh J, Kim S, Go H, Jeon YK, Chung DH. Clinicopathological analysis of PD-L1 and PD-L2 expression in pulmonary squamous cell carcinoma: comparison with tumor-infiltrating T cells and the status of oncogenic drivers. *Lung Cancer.* 2015;88:24-33.

10. Postow MA, Chesney J, Pavlick AC, et al. Nivolumab and ipilimumab versus ipilimumab in untreated melanoma. *N Engl J Med.* 2015;372:2006-2017.

11. Wolchok JD, Kluger H, Callahan MK, et al. Nivolumab plus ipilimumab in advanced melanoma. *N Engl J Med.* 2013;369:122-133.

12. Josefsson A, Nedrow JR, Park S, et al. Imaging, Biodistribution, and Dosimetry of Radionuclide-Labeled PD-L1 Antibody in an Immunocompetent mouse model of breast cancer. *Cancer Res.* 2016;76:472-479.

13. Beaino W, Nedrow JR, Anderson CJ. Evaluation of (68)Ga- and (177)Lu-DOTA-PEG4-LLP2A for VLA-4-targeted PET imaging and treatment of metastatic melanoma. *Mol Pharm.* 2015;12:1929-1938.

14. Hart IR. The selection and characterization of an invasive variant of the B16 melanoma. *Am J Pathol.* 1979;97:587-600.

15. Adiseshaiah PP, Patel NL, Ileva LV, Kalen JD, Haines DC, McNeil SE. Longitudinal imaging of cancer cell metastases in two preclinical models: a correlation of noninvasive imaging to histopathology. *Int J Mol Imaging.* 2014;2014:102702.

16. Branderhorst W, Vastenhouw B, Beekman FJ. Pixel-based subsets for rapid multi-pinhole SPECT reconstruction. *Phys Med Biol.* 2010;55:2023-2034.

17. Nedrow JR, Latoche JD, Day KE, et al. Targeting PSMA with a Cu-64 labeled phosphoramidate inhibitor for PET/CT Imaging of variant PSMA-expressing xenografts in mouse models of prostate cancer. *Mol Imaging Biol.* 2016;18:402-410.

18. Song H, Shahverdi K, Huso DL, et al. 213Bi (alpha-emitter)-antibody targeting of breast cancer metastases in the neu-N transgenic mouse model. *Cancer Res.* 2008;68:3873-3880.

19. Padda SK, Riess JW, Schwartz EJ, et al. Diffuse high intensity PD-L1 staining in thymic epithelial tumors. *J Thorac Oncol.* 2015;10:500-508.

20. Shirai T, Sano T, Kamijo F, et al. Acetylcholine receptor binding antibody-associated myasthenia gravis and rhabdomyolysis induced by nivolumab in a patient with melanoma. *Jpn J Clin Oncol.* 2016;46:86-88.

21. Palmer DB. The effect of age on thymic function. *Front Immunol.* 2013;4:316.

22. Chen K, Kolls JK. T cell-mediated host immune defenses in the lung. *Annu Rev Immunol.* 2013;31:605-633.

23. Igarashi T, Teramoto K, Ishida M, Hanaoka J, Daigo Y. Scoring of PD-L1 expression intensity on pulmonary adenocarcinomas and the correlations with clinicopathological factors. *ESMO Open.* 2016;1:e000083.

24. Taube JM, Klein A, Brahmer JR, et al. Association of PD-1, PD-1 ligands, and other features of the tumor immune microenvironment with response to anti-PD-1 therapy. *Clin Cancer Res.* 2014;20:5064-5074.

25. Hettich M, Braun F, Bartholoma MD, Schirmbeck R, Niedermann G. High-resolution PET imaging with therapeutic antibody-based PD-1/PD-L1 checkpoint tracers. *Theranostics.* 2016;6:1629-1640.

Tables

Table 1. ^{111}In-DTPA-anti-PD-L1-BC 24 hours post-injection						
Dose	MBq/nmol	mg/kg	% ID/g Tumor	% ID/g Spleen	Tumor to Blood	Tumor to Muscle
1	5.6	0.6	4.8 ± 1.7	47 ± 9.5	3.9 ± 3.0	3.2 ± 1.8
2	2.8	1.0	10 ± 2.0	26 ± 3.4	1.7 ± 0.4	9.6 ± 2.6
3	0.9	3.0	12 ± 3.0	17 ± 1.8	1.0 ± 0.2	10 ± 0.2
4	0.6	5.0	10 ± 4.4	9.0 ± 2.5	0.8 ± 0.2	8.4 ± 0.2
5	0.3	10.0	8.5 ± 1.9	6.8 ± 1.0	0.8 ± 0.1	11 ± 0.1

Table 2. ^{111}In-DTPA-anti-PD-L1-BC 72 hours post-injection						
Dose	MBq/nmol	mg/kg	% ID/g Tumor	% ID/g Spleen	Tumor to Blood	Tumor to Muscle
1	5.6	0.6	3.8 ± 0.8	23 ± 4.1	9.0 ± 2.3	2.8 ± 0.6
2	2.8	1.0	4.3 ± 0.8	21 ± 2.8	11 ± 2.3	3.1 ± 1.1
3	0.9	3.0	13 ± 6.0	21 ± 4.2	5.4 ± 2.0	8.9 ± 6.1
4	0.6	5.0	13 ± 3.0	20 ± 5.5	2.7 ± 0.9	9.3 ± 3.3
5	0.3	10.0	15 ± 8.0	12 ± 3.0	1.9 ± 1.0	8.7 ± 2.8

Figure legends

Figure 1. Flow cytometry for the murine cell lines EL4 (A), and B16F10 (B). The cells were stained with an anti-PD-L1 antibody following treatment with and without IFN-γ. Unstained cells were used as a reference.

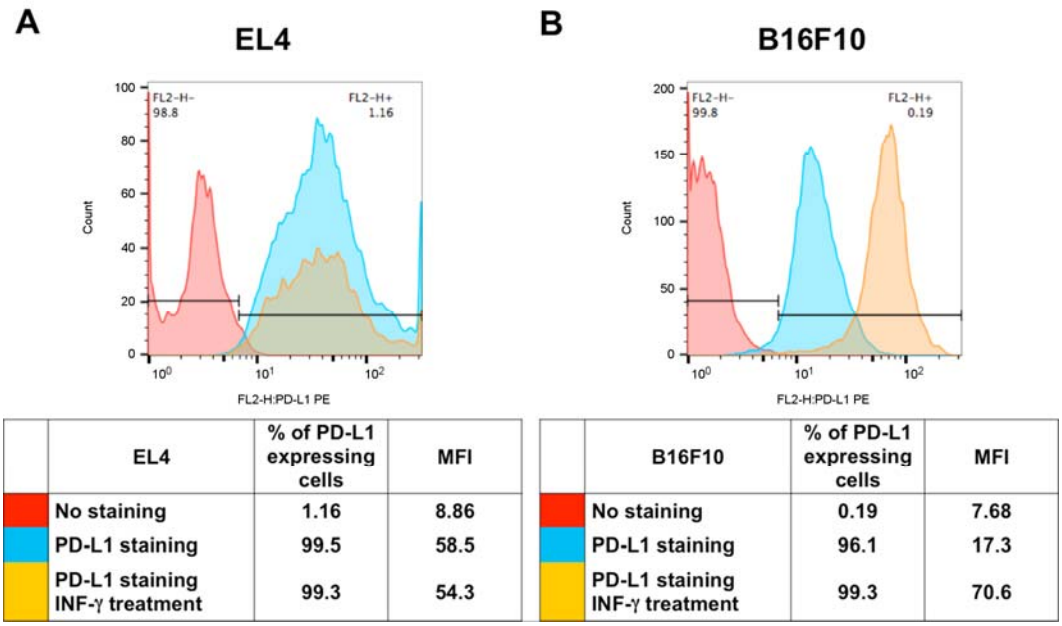

	EL4	% of PD-L1 expressing cells	MFI
	No staining	1.16	8.86
	PD-L1 staining	99.5	58.5
	PD-L1 staining INF-γ treatment	99.3	54.3

	B16F10	% of PD-L1 expressing cells	MFI
	No staining	0.19	7.68
	PD-L1 staining	96.1	17.3
	PD-L1 staining INF-γ treatment	99.3	70.6

Figure 2. Biodistribution of ^{111}In-DTPA-anti-PD-L1-BC (0.37 MBq, 0.13 mg/kg, 21.3 MBq/nmol) in B16F10 tumor-bearing mice at 1, 24, 72, and 96 hrs post-injection (n=5, except at 24 h n=4).

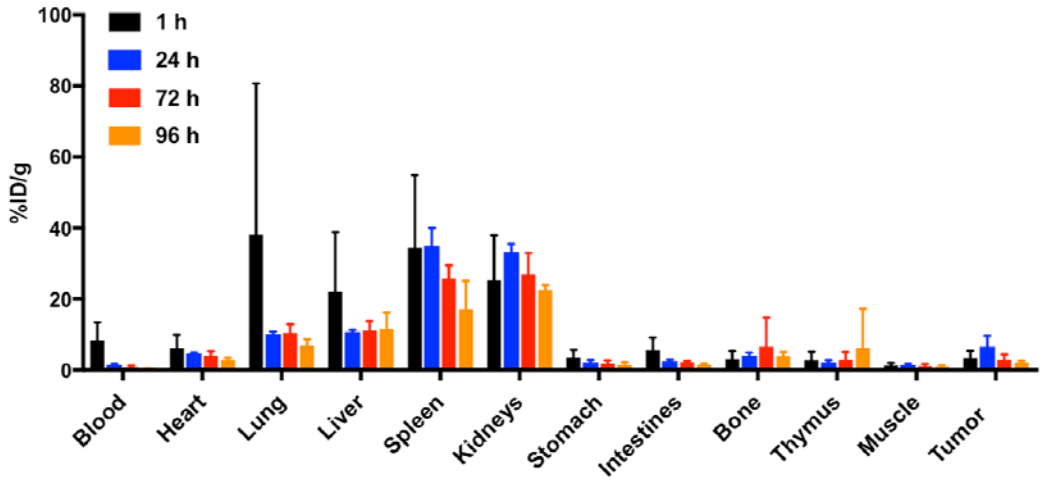

Figure 3. *Ex vivo* biodistribution of ^{111}In-DTPA-anti-PD-L1-BC at 24 (A) and 72 (C) hours post-injection in C57Bl/6 mice bearing B16F10 tumors. Dose 1. Specific Activity: 4.4 Mbq/nmol Protein Concentration: 0.6 mg/kg Dose 2. Specific Activity: 2.8 MBq/nmol Protein Concentration: 1.0 mg/kg Dose 3. Specific Activity: 0.9 MBq/nmol Protein Concentration: 3.0 mg/kg Dose 4. Specific Activity: 0.6 MBq/nmol Protein Concentration: 5.0 mg/kg Dose 5. Specific Activity: 0.3 MBq/nmol Protein Concentration: 10 mg/kg. Selected organs having significant differences in uptake between doses administered are represented in graph B for 24 hrs and D for 72 hrs. * = p ≤ 0.05, ** = p ≤ 0.01, *** = p ≤ 0.001, **** = p ≤ 0.0001.

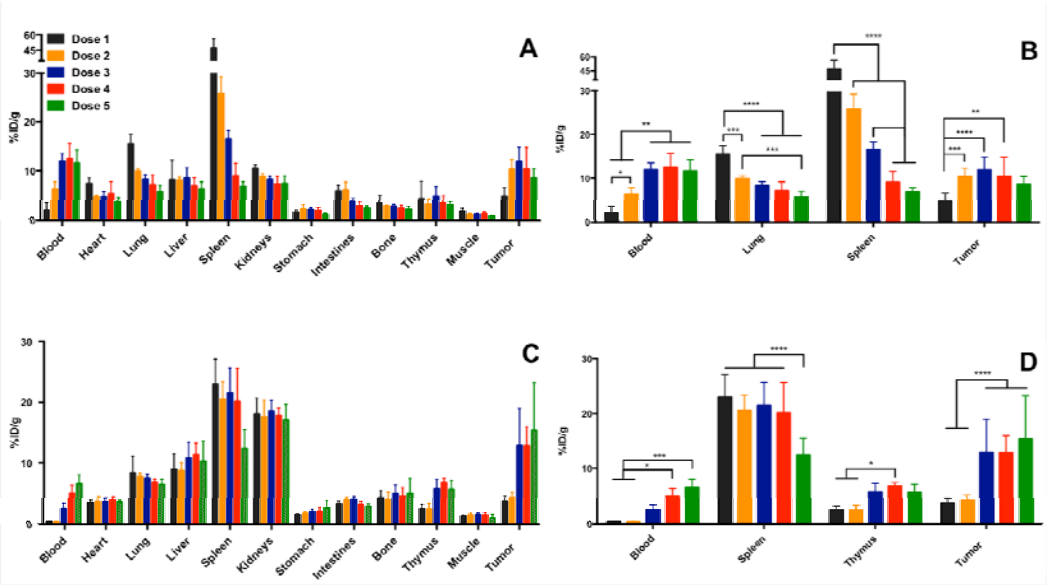

Figure 4. A coronal section of a whole-body SPECT image of ^{111}In-DTPA-anti-PD-L1-BC (3 mg/kg) 24 hrs post injection in a prone C57BL/6 mice (A &B) bearing a B16F10 tumor. Voxel intensity (MBq/ml) was calibrated from a SPECT image of a known activity and volume.

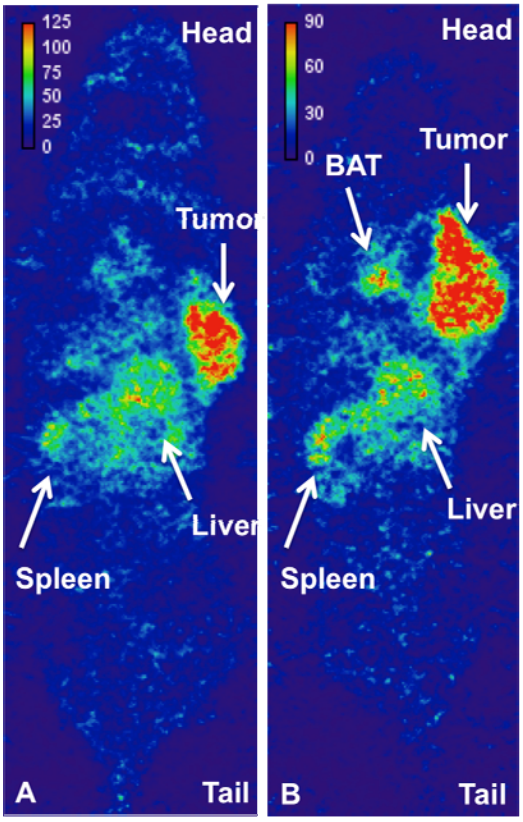

Material and methods

In vitro Studies

Cell lines

B16F10 cells were cultured on 100x20 mm^2 tissue culture dishes using heat inactivated Corning Cellgro RPMI 1640 media (Manassas, VA, USA) supplemented with 10% fetal bovine serum (FBS) and 1% penicillin-streptomycin (PS). EL4 cells were cultured with heat inactivated DMEM media supplemented with 10% horse serum. The cells were incubated at 37˚C in 5% CO_2.

Radiolabeling of DTPA-anti-PD-L1-BC antibodies with ^{111}In

The radiolabeled anti-PD-L1-BC antibody was prepared as previously described (*1*). Briefly, the antibody was conjugated to *N*-[2-amino-3-(*p*-isothiocyanatophenyl)propyl]-*trans*-cyclohexane-1,2-diamine-*N,N′*,*N′*,*N″*,*N″*-pentaacetic acid (p-SCN-Bn-DTPA) and purified by size exclusion. The resulting antibody conjugate was added to an acid washed 1.5 mL Eppendorf tube containing [^{111}In]$InCl_3$ (37-74 MBq), 0.25 mL of 0.2 M HCl and 0.03 mL of 3 M NH_4OAc, pH=7. The resulting mixture was allowed to set at room temperature for 45-60 min then purified as described previously (*2*). Radiochemical purity was determined by thin layer chromatography (TLC), and the protein concentration was determined by Nanodrop (Wilmington, DE, USA).

Western Blot Analysis

Cells were seeded in 60 mm dishes and grown to 80% confluence. The growth medium was replaced with RPMI 1640 + 1% FBS. In addition, selected plates included mouse recombinant interferon gamma (IFN-γ) 200ng/ml, EMD Millipore, Billerica, MA, USA). IFN-γ is utilized to mimic *in vivo* cell signaling that induces PD-L1 expression (*3*). The

lysates were centrifuged at 13,000 rpm for 15 min, the supernatant was collected and the protein concentration was quantified by a BCA assay. For PD-L1 expression in non-tumor-bearing C57BL/6 mice, all organs were homogenized in RIPA protein extraction buffer with freshly added proteinase inhibitors using mortar-pestle and centrifuge lysate at 12000 rpm for 15 min. The supernatant was collected and the protein concentration was determined via the BCA assay. Approximately, 40 □g of extracted cell lysates treated with and without IFN-γ and organ lysates were vertically electrophoresed on 4-12% Bis-Tris NuPAGE gel in MOPs running buffer (Invitrogen) then transferred to nitrocellulose membranes. The membranes were stained with Ponceau S stain confirming protein transfer, and blocked with 5% skim milk in PBST for 1 hr at room temperature. Membranes were washed and incubated with anti-PD-L1 antibody (1:1000, Novus Biologicals, AF1019) in 3% skim milk/PBST overnight. Following overnight incubation, the membranes were washed, incubated with a secondary antibody for 1 hr, and washed. The membranes were treated with ECL detection reagent (GE healthcare Life Sciences, Pittsburgh, PA, USA) and exposed to Hyblot CL autoradiography film to determine protein expression. The quantification of protein level was performed by densitometry scanning and normalizing to intensity of actin.

Flow cytometry

Preparation of the EL4, a positive control, and B16F10 murine cell lines were done in parallel to maintain the same treatment conditions. Flow cytometry was performed as previously described (*1*). The cell lines were seeded with growth media then serum starved for 24 hrs (1% serum). The cells were then cultured for 24 hrs with or without IFN-γ (200ng/ml). Following incubation the cells were trypsinized, washed with PBS (1x), and blocked with a 10% FBS PBS solution. Cells ($1x10^6$) were treated with anti-mouse B7-H1 (CD274)-PE clone M1H5 (Ebioscience, San Diego, CA, USA) for 30 min at 4°C.

Cells were washed (2x) and suspended in 500µl of PBS then analyzed on a FACs flow cytometer (BD Biosciences, San Jose, CA, USA).

Binding assay

The binding affinity of ^{111}In-DTPA-anti-PD-L1-BC was determined in B16F10 cells as described previously with modifications (*1,4*). Briefly, cells were seeded in 24-well plates (50,000 cells) 48 hrs prior to the experiment. IFN-γ (400 ng) was added to each well to induce PD-L1 expression. Following 24 hrs of incubation with IFN-γ cells were washed (1x) with PBS (1 mL) and 0.5 mL growth media (RPMI 1640 with 0.1% PS and 10% FBS) was added to each well. To determine non-specific binding, 5 µg of anti-PD-L1 was added to half of the wells as a cold block 30 min prior to ^{111}In-DTPA-anti-PD-L1-BC. ^{111}In-DTPA-anti-PD-L1-BC was added to all the wells in increasing concentrations (0.50–12.5 nM). The samples were incubated for 4 hrs at 4°C. After incubation, the radioactive media was removed. Wells were rinsed twice with PBS (1 mL) and the cells dissolved in 0.5% SDS solution. The radioactivity in each fraction was measured in a gamma well counter (Perkin-Elmer 2470 WIZARD^2® Automatic Gamma Counter, Waltham, MA, USA). The protein content of each cell lysate sample was determined (BCA Protein Assay Kit, Pierce). The measured radioactivity associated with the cells was normalized to the amount of cell protein present (cpm/mg protein). The K_d was calculated using PRISM 6 (GraphPad; La Jolla, CA, USA).

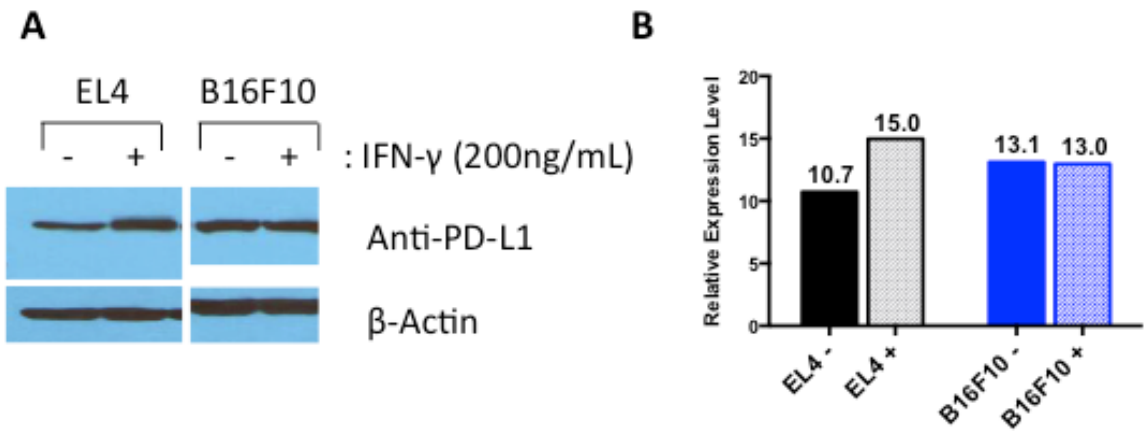

Supplemental Figure 1. PD-L1 expression was determined by western blot analysis in the EL4 and B16F10 murine cell lines, with and without IFN-γ (**A**). Expression was quantified and normalized to β-actin [PD-L1/β-actin], with and without IFN-γ (**B**).

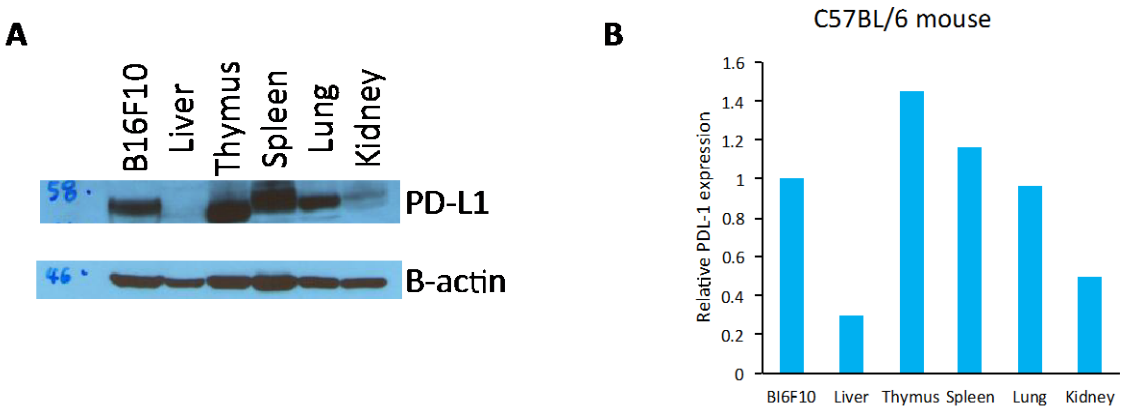

Supplemental Figure 2. PD-L1 expression in selected organs of a non-tumor-bearing C57BL/6 mouse was determined by western blot analysis with B16F10 cells serving as a positive control (**A**). Expression was quantified and normalized to β-actin [PD-L1/β-actin] and set as a ratio to expression in B16F10 cells (**B**).

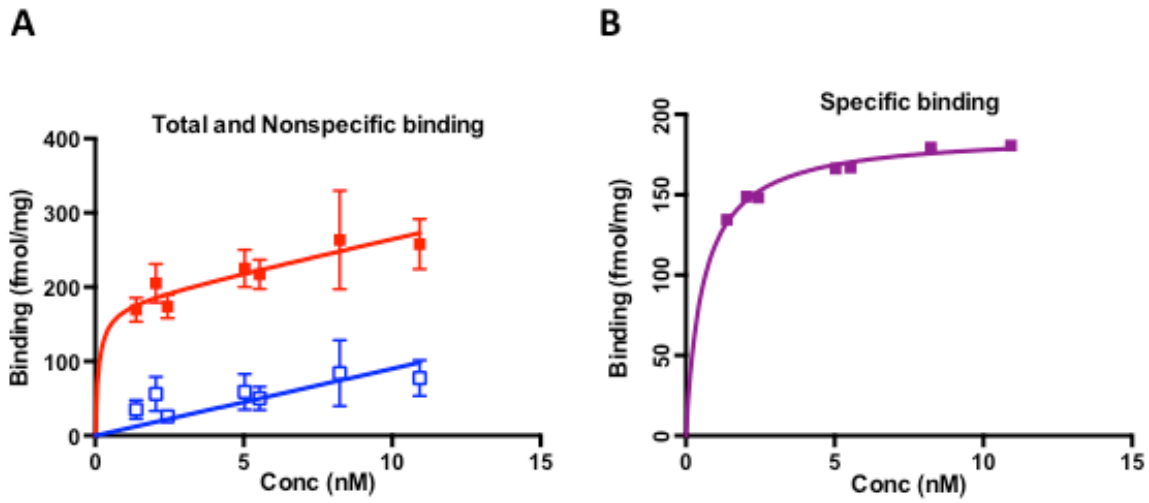

Supplemental Figure 3. Binding assays performed with ^{111}In-DTPA-anti-PD-L1-BC using B16F10 cells treated with IFN-γ (400 ng/mL). (**A**) Total [red] and Non-Specific [blue] binding. (**B**) Specific Binding [purple].

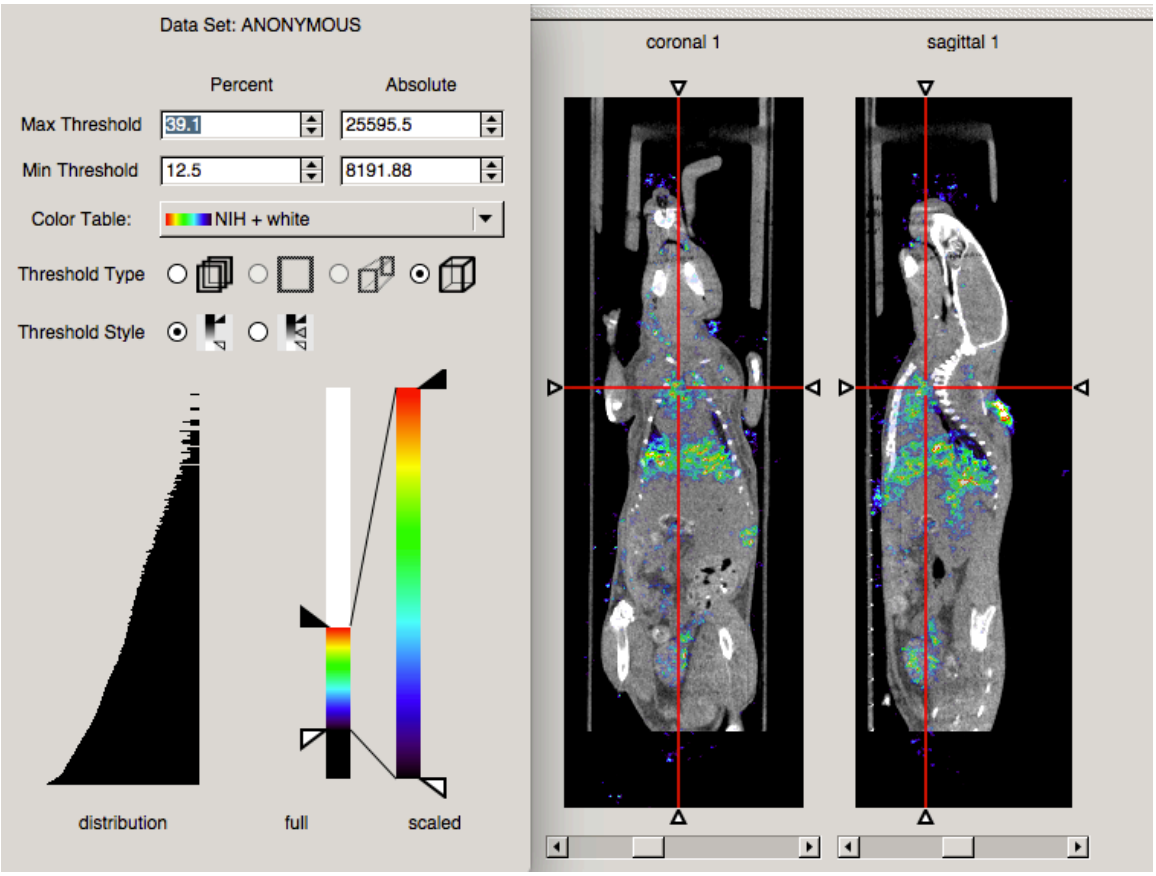

Supplemental Figure 4. A coronal and sagittal slice of a whole-body SPECT image of ^{111}In-DTPA-anti-PD-L1-BC 24 hrs post injection in a prone C57BL/6 mouse bearing a B16F10 tumor. Signal from the thymus is highlighted by the red cross arrows.

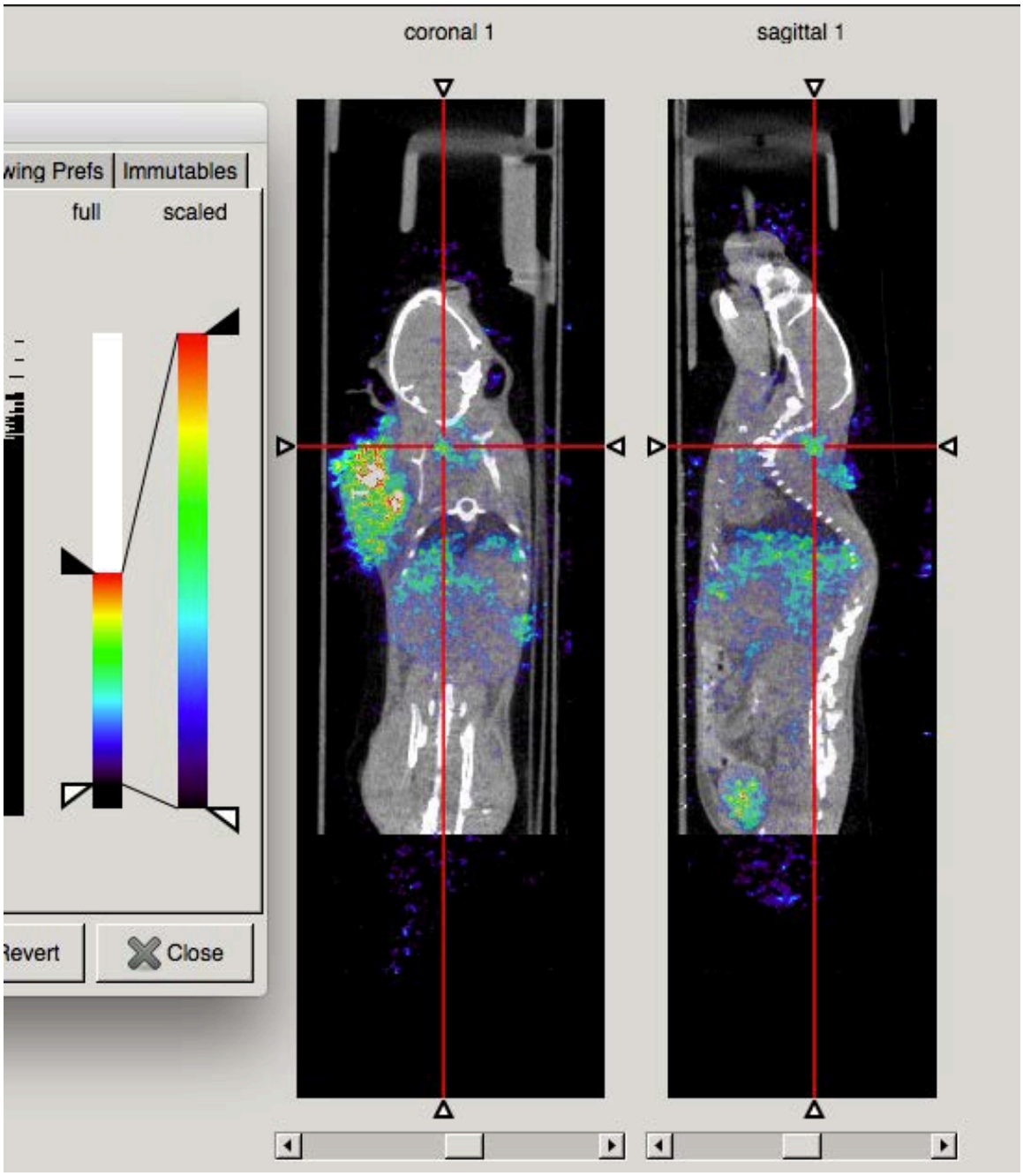

Supplemental Figure 5. A coronal and sagittal slice of a whole-body SPECT image of ^{111}In-DTPA-anti-PD-L1-BC 24 hrs post injection in a prone C57BL/6 mouse bearing a B16F10 tumor. Signal from the BAT is highlighted by the red cross arrows.

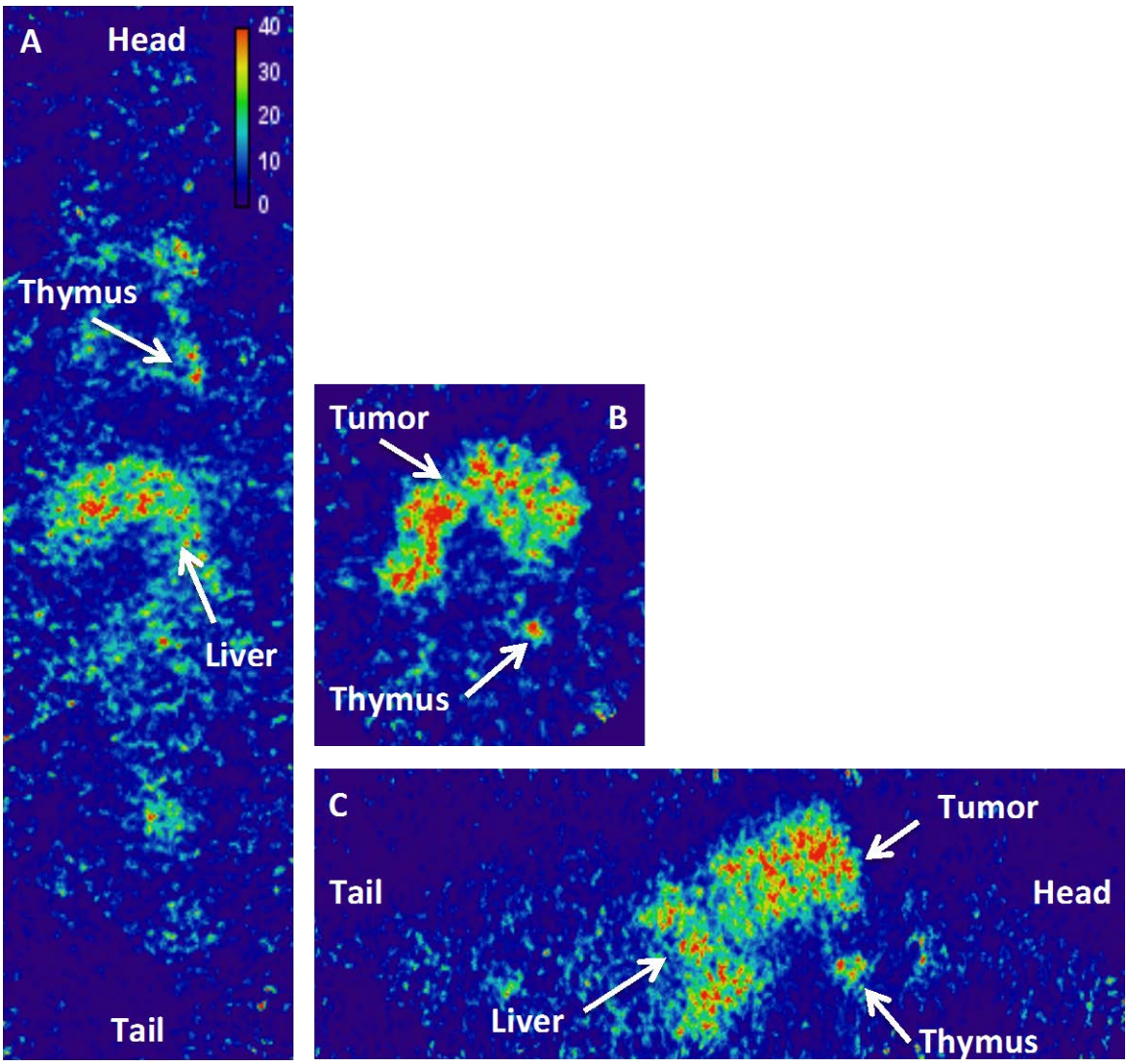

Supplemental Figure 6. A coronal (A), transverse (B), and sagittal (C) slice of a whole-body SPECT image of ^{111}In-DTPA-anti-PD-L1-BC 72 hrs post injection in a prone C57BL/6 mouse bearing a B16F10 tumor. Voxel intensity (Mbq/ml) was calibrated from a SPECT image of a known activity and volume.

REFERENCES

1. Josefsson A, Nedrow JR, Park S, et al. Imaging, Biodistribution, and Dosimetry of Radionuclide-Labeled PD-L1 Antibody in an Immunocompetent Mouse Model of Breast Cancer. *Cancer Res.* 2016;76:472-479.

2. Brechbiel MW. Bifunctional chelates for metal nuclides. *Q J Nucl Med Mol Imaging.* 2008;52:166-173.

3. Topalian SL, Drake CG, Pardoll DM. Targeting the PD-1/B7-H1(PD-L1) pathway to activate anti-tumor immunity. *Curr Opin Immunol.* 2012;24:207-212.

4. Beaino W, Nedrow JR, Anderson CJ. Evaluation of (68)Ga- and (177)Lu-DOTA-PEG4-LLP2A for VLA-4-Targeted PET Imaging and Treatment of Metastatic Melanoma. *Mol Pharm.* 2015;12:1929-1938.